Available online at www.sciencedirect.com
SCIENCE DIRECT®
Surface Science 526 (2003) 159–165
SURFACE SCIENCE
www.elsevier.com/locate/susc

# Different $CO_2$ collimation on stepped Pt(1 1 2): a comparison of NO(a) + CO(a) and O(a) + CO(a) reactions

Yu-Hai Hu [a], Song Han [b], Hideyuki Horino [b], Bernard Egbert Nieuwenhuys [a,c], Atsuko Hiratsuka [a], Yuichi Ohno [a], Kobal Ivan [d], Tatsuo Matsushima [a,*]

[a] *Catalysis Research Center, Hokkaido University, Sapporo 060-0811, Japan*
[b] *Division of Material Science, Graduate School of Environmental Earth Science, Hokkaido University, Sapporo 060-0810, Japan*
[c] *Leiden Institute of Chemistry, Gorlaeus Laboratories, Leiden University, Einsteinweg 55, P.O. Box 9502, 2300RA Leiden, The Netherlands*
[d] *Jozef Stefan Institute, 1000 Ljubljana, Slovenia*

Received 29 August 2002; accepted for publication 18 November 2002

**Abstract**

The collimation of the desorbing product $CO_2$ is very different in the NO(a) + CO(a) and O(a) + CO(a) reactions on Pt(1 1 2) = [(S)3(1 1 1) × (0 0 1)]. In the NO(a) + CO(a) reaction, $CO_2$ desorption collimated along the local normal of the (0 0 1) facets, whereas in the O(a) + CO(a) reaction, it sharply collimated close to the (1 1 1) terrace normal. This site switching is explained by different rate-determining steps.


*Keywords:* Angle resolved DIET (including electron stimulated desorption ion angular distribution (ESDIAD)); Surface chemical reaction; Platinum; Carbon monoxide; Carbon dioxide; Nitrogen molecule; Nitrogen oxides

## 1. Introduction

The spatial distributions of desorbing products provide structural information on their formation site when the products carry a high excess of translational energy, even if their emission is not rate-determining [1]. For example, the distribution in the CO oxidation changes largely when the rate-determining step switches over [2]. This paper is the first to report the angle-resolved measurements of the desorbing products $CO_2$ and $N_2$ in the NO(a) + CO(a) reaction on stepped Pt(1 1 2) = [(S)3(1 1 1) × (0 0 1)]. The collimation angle of desorbing $CO_2$ is very different from that found for the O(a) + CO(a) reaction, whereas that of $N_2$ desorption is not changed by the presence of CO(a).

The spatial distribution of the desorbing $CO_2$ produced in the O(a) + CO(a) reaction has already been reported for various platinum surfaces including stepped structures based on angle-resolved thermal desorption spectroscopy (AR-TDS) and angle-resolved steady-state desorption measurements [2,3]. Reactive $CO_2$ desorption always collimates closely along the flat terrace normal, indicating the presence of active oxygen atoms on flat (1 1 1) terraces. On Pt(1 1 3) = [(S)2(1 1 1) × (0 0 1)], $CO_2$ desorption collimated close to the

* Corresponding author. Fax: +81-11-706-3695.
*E-mail address:* tatmatsu@cat.hokudai.ac.jp (T. Matsushima).

0039-6028/02/$ - see front matter 
PII: S0039-6028(02)02597-9

(0 0 1) step normal. Originally, this result was interpreted in terms of reactive desorption from one-atom high step sites [4]. However, later LEED [5] and STM [6] results showed that the surface was reconstructed into the $(1 \times 2)$ structure as $[(S)3(1\,1\,1) \times 3(0\,0\,1)]$.

The difficulty in observing reactive $CO_2$ desorption from one-atom high step sites is due to the low reactivity of oxygen on the steps. Oxygen molecules preferentially dissociate on step sites or structural defects because of the higher binding energy [7,8]. The resultant oxygen atom is likely to be removed as $CO_2$ after moving to the flat terrace area. This is reasonable when O(a) is distributed on both step and flat terrace sites because mobile CO(a) [9], which has a surface residence time in the millisecond order [10], can visit oxygen on both sites and interact with more reactive species at ordinary steady-state reaction conditions [11]. Thus, reactive $CO_2$ desorption from the one-atom high step sites is expected when most of the O(a) is located on the steps. Such conditions are expected for the NO(a) + CO(a) reaction because NO(a) dissociation takes place on the steps at temperatures high enough to proceed the CO oxidation quickly, i.e., NO dissociation is rate-determining, being followed by the fast removal of N(a) and O(a) [12–14].

## 2. Experimental

A UHV system with three chambers was used [15]. The reaction chamber was equipped with facilities for LEED-AES, an $Ar^+$ gun, and a mass spectrometer for angle-integrated (AI) desorption analysis. The collimator house had a slit on each end and the analyzer had another mass spectrometer for AR-TDS measurements. The crystal was set on the top of a rotatable manipulator to change the desorption angle ($\theta$, polar angle). This angle was scanned in the normally directed plane perpendicular to the surface troughs because the $CO_2$ reactive desorption was concentrated in this plane [1–3]. Here, the sign of the desorption angle is defined positive in the upward direction of the steps (Fig. 1). In this definition, the (1 1 1) terrace

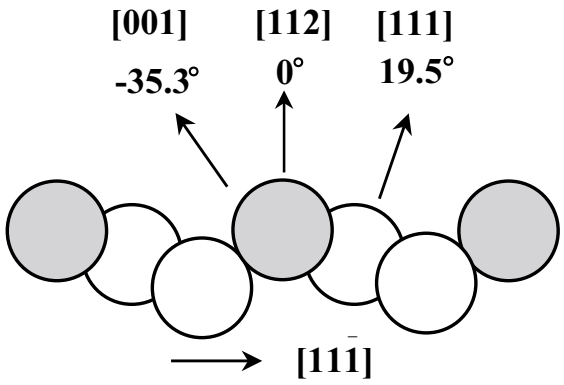


Fig. 1. A side view of Pt(1 1 2).

normal, i.e., the [1 1 1] direction, is +19.5° and the (0 0 1) step normal is −35.3°.

The crystal was cleaned by repeated cycles of $Ar^+$ bombardments and heating in oxygen. After flashing to 1200 K, the surface showed a sharp $(1 \times 1)$ LEED pattern without higher-order spots. No reactive oxygen was left on the surface as judged from the absence of $CO_2$ formation in the TDS after CO exposure. $^{15}N^{16}O$ and $^{13}C^{16}O$ were introduced through separate gas dosers when the surface temperature ($T_S$) was down to 200 K. Hereafter, the isotope $^{15}N$ and $^{13}C$ are mostly designated as N and C in the text because only $^{13}C^{16}O$ (mass/charge ratio = 29), $^{15}N_2$ (30), $^{15}N^{16}O$ (31), $^{16}O_2$ (32) and $^{13}C^{16}O_2$ (45) were desorbed in the subsequent heating procedures. The coverage of each species was defined as the AI-TDS spectrum peak area relative to its maximum value. In TDS experiments, the surface was heated at a rate of 10 K/s.

## 3. Results

### 3.1. General features

$N_2$ desorption was observed above 400 K and yielded a single $\gamma$-$N_2$ peak at around 500 K in TDS experiments after the clean surface was exposed to only NO (Fig. 2(a)) [16]. In the presence of CO(a), it was sharply enhanced at around 425 K ($\delta$-$N_2$), indicating that removal of O(a) by CO is effective for NO decomposition to proceed. A concomitant

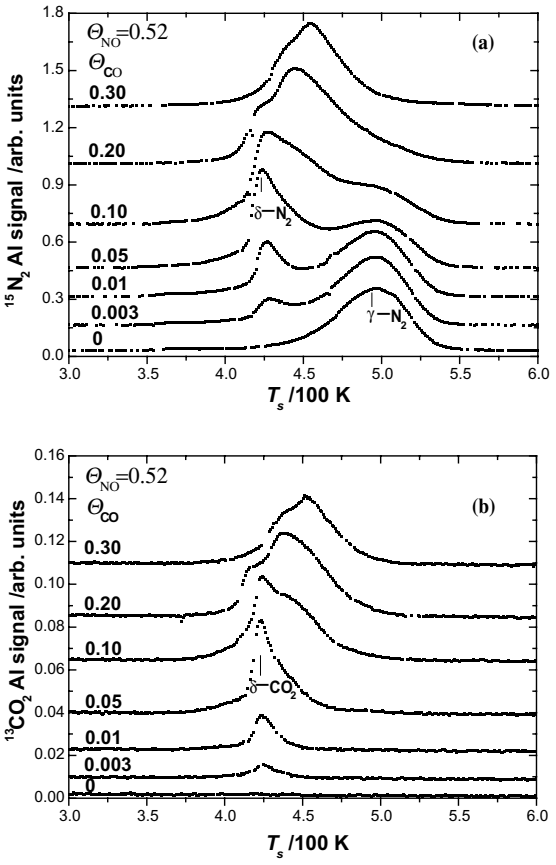


Fig. 2. Typical AI-TDS spectra of (a) $^{15}N_2$ and (b) $^{13}CO_2$ in a $^{15}NO(a)+{}^{13}CO(a)$ reaction at various $^{13}CO$ coverages. The surface was exposed to $^{15}NO$ to the amount of $\Theta_{NO}=0.52$ at 200 K and further to $^{13}CO$ in various amounts. The apparent peak areas of $^{13}CO_2$ were much fewer than those of $^{15}N_2$ because of the large difference in the pumping rate.

narrow $CO_2$ desorption peak ($\delta$-$CO_2$) was observed in the same temperature range (Fig. 2(b)), confirming the quick removal of O(a) as $CO_2$. Desorption of non-reacted oxygen was found above 700 K when the amount of CO(a) was small. CO desorption was observed only when the relative CO coverage was higher than 0.10, being consistent with the fast reaction of CO(a) with O(a) above 400 K [17].

The shape of the $N_2$ desorption curve at $\Theta_{NO}=0.52$ was sensitive to the amount of CO(a) below $\Theta_{CO}=0.10$, i.e., a small increment of adsorbed CO can enhance $N_2$ desorption around 420 K. Above this CO coverage, $N_2$ desorption shifted to higher temperatures, and the $\gamma$-$N_2$ peak at around 500 K was suppressed as well.

### 3.2. $CO_2$ angular distribution

The AR-spectra of both $N_2$ and $CO_2$ are sensitive to the desorption angle. The desorption of both species was sharply collimated around $\theta=-30°$.

Typical $CO_2$ spectra in the AR-form observed from $\Theta_{NO}=0.52$ and $\Theta_{CO}=0.05$ are summarized in Fig. 3(a). The signal was maximized at around $\theta=-30°$ and mostly suppressed in the positive desorption angle region. The peak height at 425 K is plotted against the desorption angle in the polar coordinates in Fig. 3(b). $CO_2$ desorption

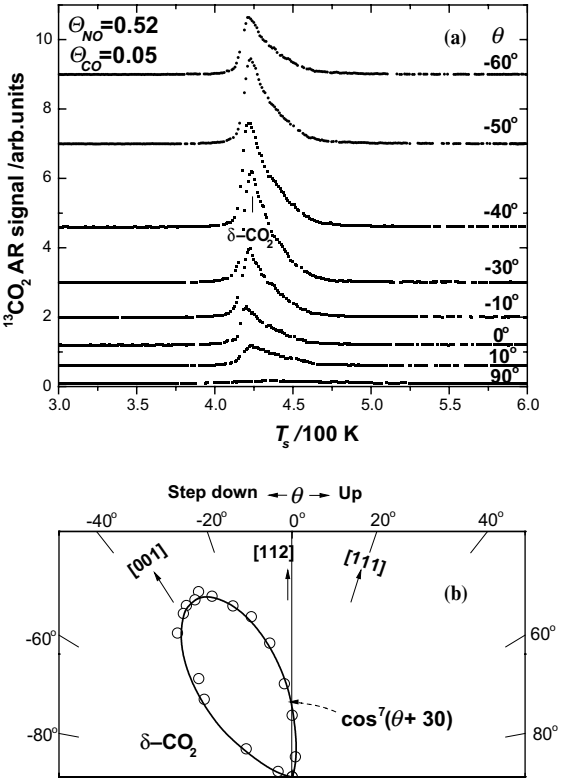


Fig. 3. (a) AR-TDS of $^{13}CO_2$ at different desorption angles in the $^{15}NO(a)+{}^{13}CO(a)$ reaction at $\Theta_{NO}=0.52$ and $\Theta_{CO}=0.05$ and (b) angular distribution of $^{13}CO_2$ in the $^{15}NO(a)+{}^{13}CO(a)$ reaction at the above condition.

collimated sharply along $\theta = -30°$. The signal can be approximated as $\cos^7(\theta + 30)$ displayed by the solid curve. The collimation angle was estimated to be $-30 \pm 2°$. It is shifted only about 5° from the [0 0 1] direction. The reactive desorption is likely to proceed on (0 0 1) facets.

This is very different from the desorption of $CO_2$ in the O(a) + CO(a) reaction on Pt(1 1 2) in our previous work [17]. For a direct comparison, the angular distribution of desorbing $CO_2$ in the O(a) + CO(a) reaction was also examined after the experiments described above. Typical AR-$CO_2$ spectra are reproduced in Fig. 4(a), where the surface was initially covered to $\Theta_O = 0.40$ and then to $\Theta_{CO} = 0.30$. The $CO_2$ formation started already at around 210 K and was completed at around 470 K, yielding three desorption peaks, $\beta_3$-$CO_2$ at 260 K, $\beta_2$-$CO_2$ at 310 K and $\beta_1$-$CO_2$ at around 400 K. The sharp $\beta_2$-peak was maximized around $\theta = +10°$ as shown in Fig. 4(b). The signal intensity can be approximated as $\cos^{13}(\theta - 10)$. On the other hand, $\beta_3$-$CO_2$ was maximized at $\theta = +5°$ and followed a $\cos^{20}(\theta - 5)$ distribution. The broad peak of $\beta_1$-$CO_2$ was maximized at around $\theta = +10°$ and approximated as $\cos^{12}(\theta - 10)$. These results agree well with our previous work [17]. $CO_2$ is formed on the terrace since its desorption is closely collimated along the (1 1 1) terrace normal.

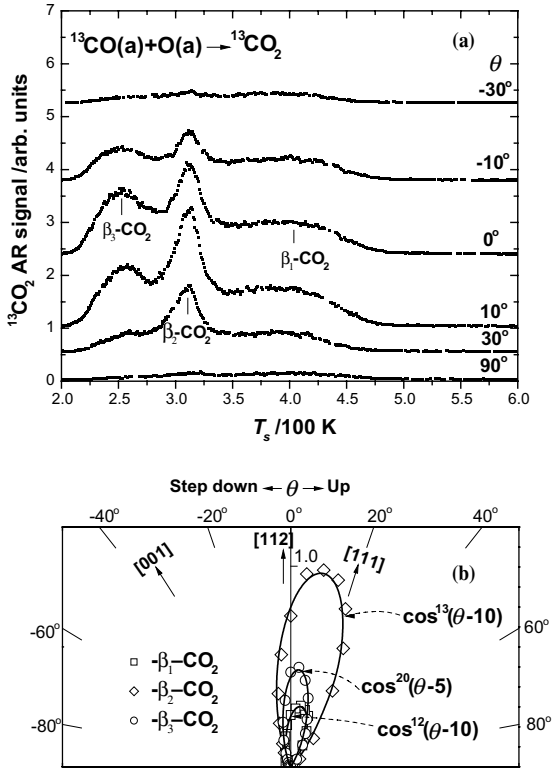


Fig. 4. (a) AR-TDS of $^{13}CO_2$ at different desorption angles in the O(a) + $^{13}$CO(a) reaction at $\Theta_{CO} = 0.30$ and $\Theta_O = 0.40$ and (b) angular distribution of $^{13}CO_2$ in the O(a) + $^{13}$CO(a) reaction. (□) $\beta_1$-$^{13}CO_2$, (◇) $\beta_2$-$^{13}CO_2$ and (○) $\beta_3$-$^{13}CO_2$. The signal intensity was normalized to the maximum value of $\beta_2$-$^{13}CO_2$.

### 3.3. $N_2$ angular distribution

The AR-spectra of $N_2$ at different desorption angles induced from $\Theta_{NO} = 0.52$ and $\Theta_{CO} = 0.05$ are summarized in Fig. 5(a). The signal was maximized at around $\theta = -30°$. It should be noted that there is a significant signal intensity at the desorption angle of $\theta = 90°$. This is due to $N_2$ molecules that did not pass through the slits directly from the surface but first desorbed into the reaction chamber and then penetrated the analyzer chamber. This extraneous signal was subtracted from the observed intensity. The apparatus was originally designed for the angle-resolved measurements of desorbing $CO_2$. The pumping rate for $CO_2$ is about 2000 l/s, high enough to reduce the $CO_2$ penetration from the reaction chamber to a negligible level. On the other hand, the pumping rate for $N_2$ was estimated to be around one twentieth of that for $CO_2$ based on the signal ratio of $CO_2$ versus $N_2$ found in the AI-form. In other words, the $N_2$ penetration from the reaction chamber to the analyzer may increase by a factor of about 20 compared with that for $CO_2$. This is why a significant $N_2$ signal is observed in the AR-form even at $\theta = 90°$ [18].

The angular distribution of $N_2$ peaks is plotted against the desorption angle in Fig. 5(b). The δ-$N_2$ desorption collimated at $\theta = -29 \pm 2°$ as $\cos^9(\theta + 29)$. The distribution became sharper from $\cos^9(\theta + 29)$ to $\cos^{14}(\theta + 30)$ with increasing the CO coverage although the collimation angle did not shift. In the absence of CO(a), $N_2$ desorbed in the range of 450–550 K, yielding the γ-$N_2$ peak at around 510 K. Its desorption followed a

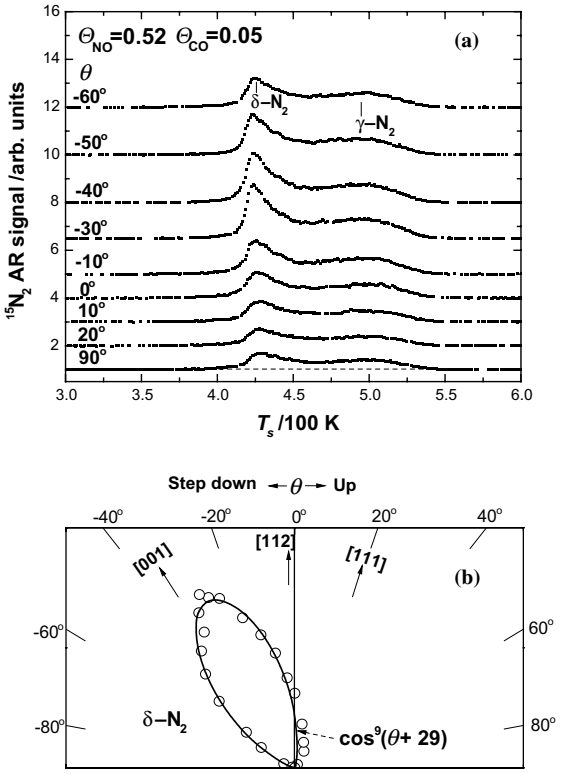


Fig. 5. (a) AR-TDS of $^{15}N_2$ at different desorption angles in the $^{15}NO(a) + {}^{13}CO(a)$ reaction at $\Theta_{NO} = 0.52$ and $\Theta_{CO} = 0.05$. (b) Angular distribution of $^{15}N_2$ in the $^{15}NO(a) + {}^{13}CO(a)$ reaction at the above condition.

$\cos^{7-8}(\theta + 30)$ form. This is similar to the collimation of around $-30°$ for $N_2$ in NO decomposition on Pd(1 1 2) reported by Ikai and Tanaka [19].

## 4. Discussion

### 4.1. Desorption mechanism

A Pt(1 1 2) surface is rather stable, compared with those of Pt(1 1 0) and Pt(1 1 3) which are easily reconstructed into a missing-row form by heating and the resultant reconstruction is lifted by adsorption of CO above a critical value. Pt(1 1 2) is stable during heating. The $(1 \times 1)$ structure is kept after CO or oxygen adsorption in a wide range of coverages [20,21].

We reported a sharp collimation of $CO_2$ desorption along $\theta = -30°$ in the NO(a) + CO(a) reaction. This angle is close to the local normal of (0 0 1) steps. As described in Section 1, when O(a) is supplied from gaseous $O_2$ in advance, desorption of the product $CO_2$ in the O(a) + CO(a) reaction collimates closely along the local normal of the (1 1 1) terrace on Pt(1 1 3) = [(S)3(1 1 1) × 3(0 0 1)], Pt(1 1 2) = [(S)3(1 1 1) × (0 0 1)], Pt(3 3 5) = [(S)4-(1 1 1) × (0 0 1)] and Pt(5 5 7) = [(S)6(1 1 1)(0 0 1)] [3]. In general, $CO_2$ is formed on oxygen adsorption sites [22], most likely on threefold hollow sites on (1 1 1) facets or on fourfold hollow sites on (0 0 1) facets [11]. In the O(a) + CO(a) reaction, CO is mostly oxidized on the threefold hollow sites because O(a) on (1 1 1) terraces has a higher reactivity [11]. The fact that the $CO_2$ reactive desorption mostly takes places on (0 0 1) facets indicates the absence of oxygen on (1 1 1) facets. This situation holds when O(a) is provided from NO dissociation on step sites at high temperatures and the subsequent removal of O(a) is very fast.

In the NO(a) + CO(a) reaction, NO(a) must be dissociated before the formation of either $N_2$ or $CO_2$. The reaction is triggered by NO(a) dissociation yielding O(a) and N(a). It is well known that NO(a) dissociates preferably on step sites [16,19]. In fact, no dissociation of NO has been found on Pt(1 1 1). Furthermore, on platinum surfaces, the combinative reaction of 2N(a) to $N_2$(g) is fast around 400 K [13] and the reaction of CO(a) with O(a) is also very fast above 400 K [3]. This is consistent with the observed concomitant desorption of δ-$N_2$ and δ-$CO_2$. The resultant products of N(a) and O(a) are likely to be first trapped on step sites and then immediately removed as $CO_2$ or $N_2$ before moving to (1 1 1) terraces. The site switching for $CO_2$ formation is controlled by the low O(a) density and its fast removal. In other words, the preference of $CO_2$ desorption from (0 0 1) steps is governed by the fact that NO dissociation on steps is rate-determining. The above mechanism can also be applied to N(a) removal.

Both γ and δ-$N_2$ desorption are commonly due to the process of $2N(a) \rightarrow N_2(g)$ and collimate along the (0 0 1) step normal. However, the desorption temperature range is different. This combinative desorption was reported to take place

on stepped Pt(3 3 5) in the range of 350–450 K after N(a) was deposited by electron bombardments [13]. This is consistent with that the δ-$N_2$ desorption at around 425 K is retarded by the slow NO dissociation. The desorption would be faster when N(a) is supplied more quickly. On the other hand, the γ-$N_2$ desorption must be more activated to proceed, suggesting that oxygen blocks sites for NO dissociation or the combination itself is retarded by the presence of O(a) because $O_2$ desorption started at around 700 K after $N_2$ desorption. This comparison suggests that δ-$N_2$ desorption takes place on oxygen-free sites formed by the fast removal of O(a).

### 4.2. Comparison with other surfaces

Ikai and Tanaka reported similar results of $N_2$ desorption in NO decomposition on Pd(1 1 2) in the absence and presence of gaseous hydrogen [19]. $N_2$ desorption peaked at 480–500 K and collimated at around −30° off the surface normal. Using labeled N, it was shown that $N_2$ was formed as $^{15}N(a) + {}^{14}NO(a) \rightarrow {}^{15}N^{14}N$. Although the authors did not argue this point, their result strongly suggests that $N_2O(a)$ is the intermediate of desorbing $N_2$ in a similar way to Pd(1 1 0) [23] because of the concomitant formation of the byproduct $N_2O$. This byproduct is formed within the same temperature range as $N_2$ desorption and is quickly decomposed at around the temperature of NO dissociation, yielding $N_2$. In fact, $N_2$ is merely desorbed through $N_2O$ dissociation in the thermal NO decomposition on Pd(1 1 0) at lower temperatures [23]. The $N_2$ emission on palladium may proceed through $N_2O$ dissociation on (0 0 1) steps. A similar $N_2$ emission is also possible on Rh(3 3 5) where $N_2$ desorption was reported to collimate at −15° off the surface normal [24]. This is fairly at the middle of the (1 1 1) terrace normal of +14.1° and the (0 0 1) step normal of −40.3°. $N_2O(a)$ is likely to be easily dissociated at around 100–150 K on palladium and rhodium surfaces [25]. Spatial distribution measurements of $N_2$ in $N_2O$ decomposition might be useful to differentiate the above associative mechanism from the $N_2O$ decomposition pathway. On Pt(1 1 2), $N_2$ desorption may proceed through the associative reaction of N(a) because no $N_2O$ is found in NO decomposition. However, the contribution from the $N_2O$ decomposition pathway is not completely ruled out since $N_2O$ dissociation proceeds on Pt(1 1 2) at 120–140 K [26].

## Acknowledgements

Y.-H. Hu is supported by JSPS (The Japanese Society for the Promotion of Science) Fellowship Programs for Foreign Researchers for research in Japan in the period 2001–2003. S. Han is indebted to the Clark Memorial Foundation in the period 2002–2003. I. Kobal was supported by the scientist exchange program between JSPS and the Ministry of Education, Science, and Sport of Slovenia in 2002. This work was partly supported by Grant-in-Aid no. 13640493 for General Scientific Research from JSPS.

## References

[1] I. Kobal, T. Matsushima, Trends Chem. Phys. 7 (1999) 169.
[2] I. Kobal, I. Rzeznicka, T. Matsushima, in: Recent Developments of Physical Chemistry, Transworld Research Network, in press.
[3] T. Matsushima, Heterogen. Chem. Rev. 2 (1995) 51.
[4] T. Yamanaka, C. Moise, T. Matsushima, J. Chem. Phys. 107 (1997) 8138.
[5] R. Kose, D.A. King, Chem. Phys. Lett. 313 (1999) 1.
[6] T. Yamanaka, Q.K. Xue, K. Kimura, T. Matsushima, Y. Hasegawa, T. Sakurai, Jpn. J. Appl. Phys. 39 (2000) 3562.
[7] A. Rar, T. Matsushima, Surf. Sci. 318 (1994) 89.
[8] H. Wang, R.G. Tobin, D.K. Lambert, C.L. DiMaggio, G.B. Fisher, Surf. Sci. 372 (1997) 267.
[9] J.E. Reutt-Robey, D.J. Doren, Y.J. Chabal, S.B. Christman, Phys. Rev. Lett. 61 (1988) 2778.
[10] C.T. Campbell, G. Ertl, H. Kuipers, J. Segner, J. Chem. Phys. 73 (1980) 5862.
[11] G.Y. Cao, G. Moula, Y. Ohno, T. Matsushima, J. Phys. Chem. B 103 (1999) 3235.
[12] Y.O. Park, W.F. Banholzer, R.I. Masel, Surf. Sci. 155 (1985) 341.
[13] H. Wang, R.G. Tobin, C.L. DiMaggio, G.B. Fisher, D.K. Lambert, J. Chem. Phys. 107 (1997) 9569.
[14] R.D. Ramsier, Q. Gao, H.N. Waltenburg, J.T. Yates Jr., J. Chem. Phys. 100 (1994) 6837.

[15] T. Matsushima, Surf. Sci. 127 (1983) 403.
[16] T. Sugisawa, J. Shiraishi, D. Machihara, K. Irokawa, H. Miki, C. Kodama, T. Kuriyama, T. Kubo, H. Nozoye, Appl. Surf. Sci. 169–170 (2001) 292.
[17] A. Rar, H. Sugimura, A. Barrera, Y. Ohno, T. Matsushima, Surf. Sci. 348 (1996) 77.
[18] M. Kobayashi, Y. Tuzi, J. Vac. Sci. Technol. 16 (1979) 685.
[19] M. Ikai, K. Tanaka, J. Chem. Phys. 110 (1999) 7031.
[20] M.A. Henderson, A. Szabo, J.T. Yates Jr., J. Chem. Phys. 91 (1989) 7245.
[21] A. Szabo, M.A. Henderson, J.T. Yates Jr., J. Chem. Phys. 96 (1992) 6191.
[22] A. Alavi, P.J. Hu, T. Deutsch, P.L. Silvestrelli, J. Hutter, Phys. Rev. Lett. 80 (1998) 3650.
[23] Y. Ohno, K. Kimura, M. Bi, T. Matsushima, J. Chem. Phys. 110 (1999) 8221.
[24] M. Ikai, N.M.H. Janssen, B.E. Nieuwenhuys, K. Tanaka, J. Chem. Phys. 106 (1997) 311.
[25] H. Horino, I. Rzeznicka, A. Kokalj, I. Kobal, Y. Ohno, A. Hiratsuka, T. Matsushima, J. Vac. Sci. Technol. A 20 (2002) 1592.
[26] Y. Hu, unpublished data.